



LIMIT STATE ANALYSIS OF FIXED-HEAD CONCRETE PILES UNDER LATERAL LOADS

S. T. SONG¹, Y. H. CHAI² & Tom H. HALE³

SUMMARY

Under seismic loads, deep foundations with fixed pile/pile-cap connection may be subjected to a large curvature demand at the pile head. Damage induced by local inelastic deformation depends on the magnitude of the lateral displacement imposed on the pile. In this paper, an analytical model relating the displacement ductility factor to the local curvature ductility demand is proposed for fixed-head piles embedded in cohesive and cohesionless soils. The model indicates that the curvature ductility demand depends on the strength and stiffness of the soil-pile system, as well as the location and length of the plastic hinges. The model is useful for design of fixed-head piles since it is capable of estimating the severity of the local damage in the pile for a wide range of pile and soil properties. The versatility of the model is illustrated using an example of a fixed-head concrete pile constructed in soil types currently classified in the US building codes. Seismic performance of the pile subjected to displacement ductility factor commensurate with the current design is assessed for different soil conditions.

INTRODUCTION

Deep foundations for buildings and bridges often rely on the use of concrete piles that are restrained from rotation at the pile head. Under lateral seismic loads, however, the fixity at the pile/pile-cap connection induces a large curvature demand at the pile head, with a potential for failure in the pile. Severe damage of pile-supported foundations had been observed in recent earthquakes. As post-earthquake inspection of pile foundations is difficult, damage assessment of piles becomes important, particularly if a certain level of performance is to be guaranteed for the structure.

For a fixed-head pile subjected to a large lateral load, sequential yielding of the pile occurs until a plastic mechanism is fully developed. Figure 1 shows the deflected shape and the associated bending moment distribution at various limit states of a laterally loaded fixed-head pile. The first yield limit state of the pile, which is shown in Figure 1(a), is characterized by a maximum bending moment at the pile/pile-cap

¹ Graduate Research Assistant, Dept. of Civil & Environ. Engr., UC Davis, California, USA.
E-mail: ssong@ucdavis.edu

² Associate Professor, Dept. of Civil & Environ. Engr., UC Davis, California, USA. E-mail: yhchai@ucdavis.edu

³ Senior Structural Engineer, Office of Statewide Health Planning and Development, Sacramento, California, and
Chair of the SEAOC Central Seismology Committee, USA. E-mail: THale@oshpd.state.ca.us

connection where the flexural strength M_u of the pile is reached. A plastic hinge is then assumed to form at the pile head with the center of rotation occurring at the ground level. Further displacement beyond the first yield limit state involves a concentrated rotation of the plastic hinge, which is accompanied by a redistribution of internal forces in the pile. The redistribution increases the bending moment in the non-yielding portion of the pile until the formation of a second plastic hinge. Figure 1(b) shows the second yield limit state where the second plastic hinge forms at a depth L_m . Continued lateral displacement after the second plastic hinge formation is facilitated by inelastic rotations in both plastic hinges until the pile reaches the ultimate limit state, as shown in Figure 1(c). The ultimate limit state is assumed to be associated with a flexural failure, as dictated by a limiting curvature in the plastic hinge. In order to control the damage due to flexural yielding of the pile, the curvature ductility demand in the pile from an imposed lateral displacement must be properly assessed. A simple mechanistic model is developed in subsequent sections for characterizing the lateral response of fixed-head piles for various limit states. The model is capable of predicting the lateral stiffness and lateral strength of the pile as well as the curvature ductility demand in the pile.

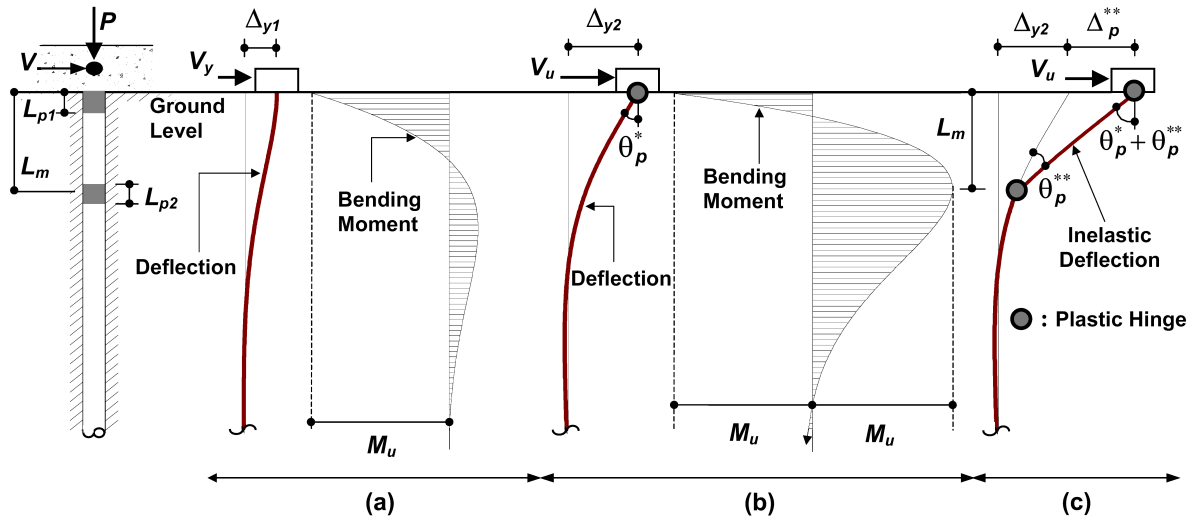


Figure 1. Deflected shape and bending moment distribution of a laterally loaded fixed-head pile (a) first yield limit state, (b) second yield limit state, and (c) ultimate limit state.

ANALYTICAL MODEL

Satisfactory seismic performance of fixed-head piles depends on the level of inelastic deformation imposed on the pile. Inelastic deformation, as commonly characterized in terms of curvature demand, is related to the stiffness and strength of the soil-pile system as well as the plastic hinge length of the pile. In this section, a kinematic model, which relates the displacement ductility factor to the curvature ductility factor, is derived. The model is developed for different soil conditions.

Lateral Stiffness of Soil-Pile System: Cohesive Soils

A common approach for seismic design of pile foundations assumes that a laterally loaded soil-pile system can be analyzed as a flexural member supported by an elastic Winkler foundation. In this case, the soil is replaced by a series of springs, which provide a soil reaction that is proportional to the lateral deflection. For cohesive soils, the stiffness of the soil-spring is assumed to be independent of the depth, resulting in a constant horizontal subgrade reaction k_h (in units of force/length³) for the Winkler foundation. Closed-form solutions for the deflection and bending moment of an elastic pile embedded in cohesive soils are

well known [1]. For a fixed-head pile with an imposed lateral displacement Δ at the ground level, the lateral stiffness of the soil-pile system is given by

$$K_1 \equiv \frac{V}{\Delta} = \sqrt{2} \frac{EI_e}{R_c^3} \quad (1)$$

where V is the lateral force required to produce an elastic displacement Δ , EI_e is the effective flexural rigidity of the pile, and R_c is the characteristic length of the pile, which is defined as $R_c \equiv \sqrt[4]{EI_e/k_h}$. At the first yield limit state, the lateral deflection Δ_{y1} at the ground level can be obtained by equating the bending moment at the pile/pile-cap connection to the ultimate moment capacity M_u of the pile, assuming an elasto-plastic moment-curvature response i.e.

$$\Delta_{y1} = \frac{M_u R_c^2}{EI_e} \quad (2)$$

Using the lateral stiffness K_1 of Eq. (1) and the yield displacement Δ_{y1} of Eq. (2), the lateral force to cause the formation of the first plastic hinge is:

$$V_y = K_1 \Delta_{y1} = \sqrt{2} \frac{M_u}{R_c} \quad (3)$$

Upon the formation of the first plastic hinge, the boundary condition of the pile effectively changes to a free-head condition, where closed-form solutions are also readily available. The reduced lateral stiffness K_2 and the corresponding plastic rotation θ at the ground level after the first yield limit state are given by:

$$K_2 \equiv \frac{V - V_y}{\Delta - \Delta_{y1}} = \frac{EI_e}{\sqrt{2} R_c^3} \quad \text{for } V > V_y \text{ and } \Delta > \Delta_{y1} \quad (4)$$

$$\theta = \frac{\Delta - \Delta_{y1}}{\sqrt{2} R_c} \quad \text{for } \Delta > \Delta_{y1} \quad (5)$$

The lateral stiffness of fixed-head piles embedded in cohesive soils requires the determination of the characteristic length R_c of the pile, which in turn requires an estimation of the modulus of horizontal subgrade reaction k_h . An expression for k_h has been proposed by Davisson [2] for estimating the modulus of horizontal subgrade reaction of cohesive soils:

$$k_h = 67 s_u \quad (6)$$

where s_u is the undrained shear strength of the cohesive soil, which may be determined from field tests or from site classifications in current US building codes. For example, NEHRP [3] or ATC-40 [4] provides a correlation between the undrained shear strength and soil profile type, which is reproduced in Table 1 for completeness of this paper.

Table 1. Soil profile classifications and soil properties (adapted from NEHRP [3] and ATC-40 [4])

Soil profile	Description	Shear wave velocity (m/sec)	SPT N (blows/0.305m)	Cohesive soils	Cohesionless soils
				Undrained shear strength (kN/m ²)	Friction angle $\bar{\phi}$ (degrees)
S_E	Soft soil	< 180	< 15	< 50	< 33
S_D	Stiff soil	180 – 360	15 – 50	50 – 100	33 – 40
S_C	Dense soil	360 - 760	> 50	> 100	> 40

Lateral Stiffness of Soil-Pile System: Cohesionless Soils

The above approach for determining the lateral stiffness of fixed-head piles can be extended to piles embedded in cohesionless soils. In this case, the soil resistance is modeled by a Winkler foundation with a linearly increasing modulus of horizontal subgrade reaction. Solutions for estimating the deformation and bending moment of elastic piles in cohesionless soils have been proposed by Matlock and Reese [5]. For a fixed-head pile, the lateral stiffness of the soil-pile system is given by:

$$K_1 \equiv \frac{V}{\Delta} = 1.08 \frac{EI_e}{R_n^3} \quad (7)$$

where R_n is the characteristic length, which is defined as $R_n \equiv \sqrt[3]{EI_e / n_h}$ for cohesionless soils, and n_h is the constant rate of increase of the modulus of horizontal subgrade reaction (in units of force/length³). At the first yield limit state, the lateral deflection and force at the ground level, denoted as Δ_{y1} and V_y respectively, are given by:

$$\Delta_{y1} = \frac{M_u R_n^2}{EI_e} \quad (8)$$

$$V_y = K_1 \Delta_{y1} = 1.08 \frac{M_u}{R_n} \quad (9)$$

Similar to the case for cohesive soils, the reduced stiffness K_2 after the first yield limit state and its corresponding rotation at ground level for piles in cohesionless soils are:

$$K_2 \equiv \frac{V - V_y}{\Delta - \Delta_{y1}} = 0.41 \frac{EI_e}{R_n^3} \quad \text{for } V > V_y \text{ and } \Delta > \Delta_{y1} \quad (10)$$

$$\theta = \frac{2}{3} \frac{\Delta - \Delta_{y1}}{R_n} \quad \text{for } \Delta > \Delta_{y1} \quad (11)$$

The lateral stiffness of a pile embedded in cohesionless soils depends on the rate of increase of modulus of horizontal subgrade reaction n_h . An estimation of n_h and its correlation with the effective friction angle and relative density of the soil is suggested in ATC-32 [6] and is reproduced in Figure 2 in this paper. Note that Table 1, which is adopted from ATC-40 [4], also provides a correlation between the friction angle and the soil profile classifications by NEHRP [3].

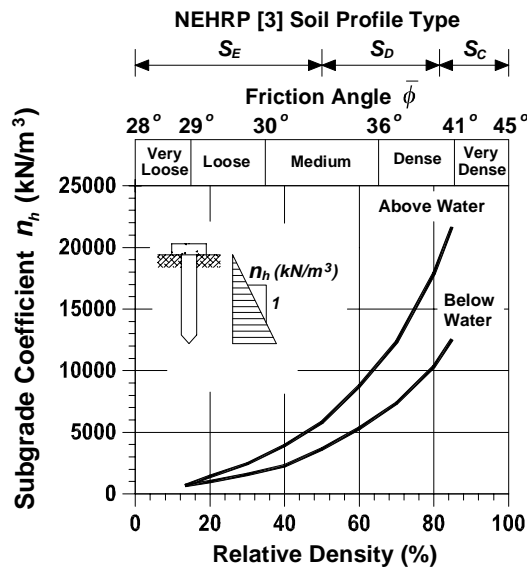


Figure 2. Subgrade coefficient of cohesionless soils [6]

Lateral Strength of Soil-Pile System: Cohesive Soils

For a laterally loaded fixed-head concrete pile, the response may be assumed to be characterized by a dependable lateral strength with a varying level of ductility capacity, depending on the level of confinement provided for the pile. The lateral strength of the pile can be determined by assuming that a sufficiently large deflection has occurred so that an ultimate soil pressure, extending to the depth of the maximum bending moment, is fully developed. The depth to the maximum bending moment, which depends on the flexural strength of the pile and the ultimate pressure of the soil, defines the location of the second plastic hinge and therefore influences the lateral strength and ductility of the pile.

The magnitude and distribution of the ultimate soil pressure acting on the pile depend on the failure mechanism of the soil, the shape of the pile cross-section, the friction between the pile surface and surrounding soil, etc. For cohesive soils, an estimation of the ultimate soil pressure distribution may be obtained from consideration of a failure mechanism of the soil around the pile, as suggested by Reese and Van Impe in [7]. The failure mechanism in the upper region is controlled by a sliding soil wedge resulting in a soil pressure that increases linearly with depth, while a plastic flow occurs around the pile in the lower region leading to a constant ultimate lateral pressure. Using such failure mechanism, the ultimate soil pressure distribution of cohesive soils may be written as:

$$p_u(x) = \begin{cases} \left(2 + \frac{9}{\psi_r} \frac{x}{D}\right) s_u & \text{for } x \leq x_r \\ 11s_u & \text{for } x > x_r \end{cases} \quad (12)$$

The depth delineating the two regions is defined as the critical depth x_r , which varies with the undrained shear strength and is given by

$$x_r \equiv \psi_r D = \frac{9s_u}{\gamma' D + 2\sqrt{2}s_u} D \quad (13)$$

where ψ_r is the critical depth coefficient and γ' is the effective unit weight of the soil. The ultimate soil pressure distribution of Eq. (12) is plotted in Figure 3(a) and will be used for calculating the lateral strength of fixed-head piles embedded in cohesive soils.

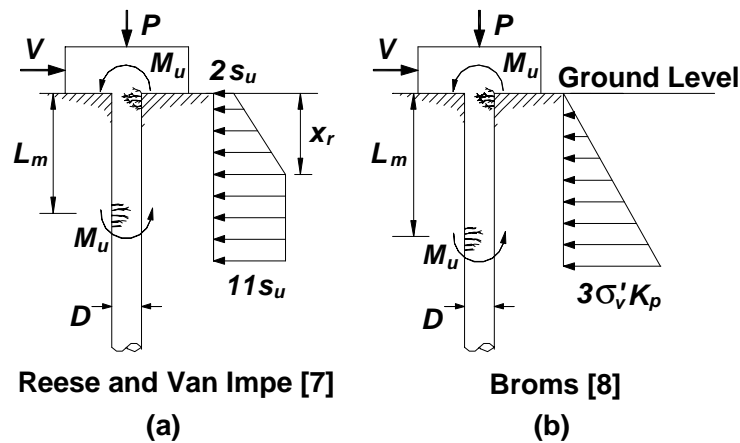


Figure 3. Ultimate soil pressure distribution for laterally loaded fixed-head piles: (a) cohesive soils, (b) cohesionless soils.

The depth at which the second plastic hinge forms L_m and the ultimate lateral strength of the soil-pile system V_u can be determined using the equilibrium condition for lateral force and bending moment. For cohesive soils with an ultimate pressure distribution given by Eq. (12), the normalized depth to the second plastic hinge, defined as $L_m^* \equiv L_m / D$, is given by the solution of the equation:

$$M_u^* = \begin{cases} \frac{1}{2} L_m^{*2} + \frac{3}{2} \frac{L_m^{*3}}{\psi_r} & \text{for } L_m^* \leq \psi_r \\ \frac{11}{4} L_m^{*2} - \frac{3}{4} \psi_r^2 & \text{for } L_m^* > \psi_r \end{cases} \quad (14)$$

where $M_u^* \equiv M_u / (s_u D^3)$ is the normalized flexural strength of the pile. Upon the determination of the normalized depth to the second plastic hinge, the normalized lateral strength V_u^* can be obtained by

$$V_u^* = \begin{cases} 2L_m^* + \frac{9}{2} \frac{L_m^{*2}}{\psi_r} & \text{for } L_m^* \leq \psi_r \\ 11L_m^* - \frac{9}{2} \psi_r & \text{for } L_m^* > \psi_r \end{cases} \quad (15)$$

where the normalized lateral strength is defined as $V_u^* \equiv V_u / (s_u D^2)$.

Lateral Strength of Soil-Pile System: Cohesionless Soils

The lateral strength, as well as the depth to the second plastic hinge, of a fixed-head pile embedded in a cohesionless soil can be determined similarly to that for cohesive soils. Studies on the magnitude and distribution of the ultimate soil pressure on piles in cohesionless soils have been made in the past, and an ultimate lateral pressure distribution that is convenient for design has been proposed by Broms [8]. The lateral pressure p_u on the pile is taken to be equal to 3 times the Rankine passive pressure of the soil:

$$p_u(x) = 3 \sigma'_v(x) K_p \quad (16)$$

where $\sigma'_v(x)$ is the vertical effective overburden stress, which may be taken as the effective unit weight γ' multiply by the depth x , and the term K_p is the coefficient of passive soil pressure and is given by

$$K_p = \frac{(1 + \sin \bar{\phi})}{(1 - \sin \bar{\phi})} \quad (17)$$

where $\bar{\phi}$ is the friction angle of the cohesionless soil. The ultimate pressure distribution of Eq. (16), which varies linearly with depth, is shown in Figure 3(b).

The depth at which the second plastic hinge forms L_m and the ultimate lateral strength of the soil-pile system V_u can be determined using the ultimate soil pressure distribution of Eq. (16). The normalized depth to the second plastic hinge, defined as $L_m^* \equiv L_m / D$, and the normalized ultimate strength, defined as $V_u^* \equiv V_u / (K_p \gamma' D^3)$, for piles in cohesionless soils, are given by:

$$L_m^* = \sqrt[3]{2 M_u^*} \quad (18)$$

$$V_u^* = \frac{3}{2} L_m^{*2} \quad (19)$$

where the normalized flexural strength M_u^* is defined as $M_u^* \equiv M_u / (K_p \gamma' D^4)$.

Kinematic Relation between Displacement and Curvature Ductility Factors

To ensure a satisfactory performance, the severity of local damage may be controlled by limiting the curvature ductility demand in the potential plastic hinge region. The curvature ductility demand, which is different for the two plastic hinges, depends on the displacement ductility imposed on the pile. In order to estimate the local inelastic deformation and hence the curvature ductility demand in the critical region, the lateral response of a fixed-head pile is approximated by a tri-linear force-displacement response, as shown in Figure 4, with an initial stiffness K_1 followed by a reduced stiffness K_2 . The first and second yield limit states are defined by the lateral displacement Δ_{y1} and Δ_{y2} , respectively. The lateral displacement beyond Δ_{y2} is characterized by a constant lateral force signifying a fully plastic response. The ultimate limit state is defined by the lateral displacement Δ_u , which depends on the ductility capacity of the plastic hinges. The lateral force-displacement response of the fixed-head pile can be further idealized by a bilinear elasto-plastic response, which is also shown in Figure 4, with the equivalent elasto-plastic yield displacement Δ_y . Herein the displacement ductility factor μ_Δ is defined as

$$\mu_\Delta \equiv \frac{\Delta_u}{\Delta_y} = \frac{\Delta_{y2}}{\Delta_y} + \frac{\Delta_p^{**}}{\Delta_y} \quad (20)$$

where Δ_p^{**} is the increased plastic displacement from the stage of second plastic hinge formation to the ultimate limit state, as indicated in Figure 4. The relation between the displacement and curvature ductility factors can be established by formulating Eq. (20) as a function of the yield and ultimate curvatures of the pile section.

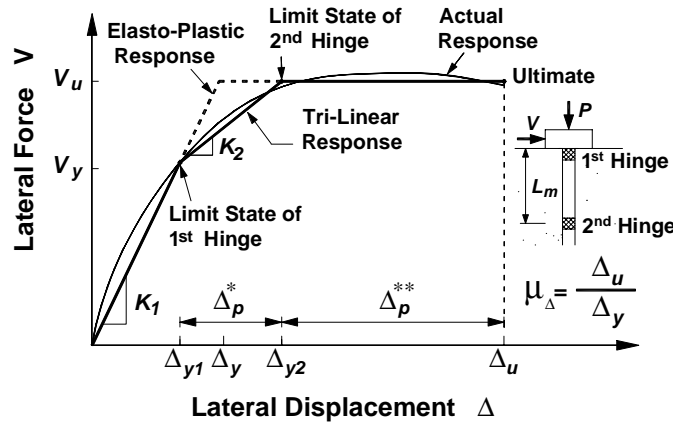


Figure 4. Idealized lateral force-displacement response of fixed-head piles

The equivalent elasto-plastic yield displacement Δ_y in Eq. (20) may be related to the ultimate lateral strength V_u using the initial stiffness K_1 of the bilinear curve:

$$\Delta_y = \frac{V_u}{K_1} \quad (21)$$

while the lateral displacement at the second yield limit state Δ_{y2} in Eq. (20) may be determined from the idealized tri-linear response, i.e.:

$$\Delta_{y2} = \frac{V_y}{K_1} + \frac{V_u - V_y}{K_2} \quad (22)$$

where V_y is the lateral force required to develop the first plastic hinge. The next step of the formulation involves the determination of the plastic rotation for both hinges. The lateral displacement of the pile from Δ_{y2} to Δ_u results in a rotation of θ_p^{**} in both plastic hinges. The plastic hinge rotation θ_p^{**} is related to the plastic displacement Δ_p^{**} , as shown in Figure 1(c), by

$$\theta_p^{**} = \frac{\Delta_p^{**}}{L_m} \quad (23)$$

where $L_m = L_m^* D$ is the depth to the second plastic hinge. In order to estimate the curvature ductility, the plastic rotation is taken to be uniformly distributed over the plastic hinge. For the first plastic hinge, the plastic rotation θ_p^{**} can be written as

$$\theta_p^{**} = (\phi_{u1} - \phi_i) L_{p1} \quad \text{for } \phi_{u1} \geq \phi_i \geq \phi_y \quad (24)$$

where ϕ_i is the curvature in the first plastic hinge at the lateral displacement Δ_{y2} , ϕ_{u1} is the ultimate curvature in the first plastic hinge, and L_{p1} is the equivalent plastic hinge length for the first hinge. By normalizing the first plastic hinge length to $\lambda_{p1} \equiv L_{p1} / D$, the combination of Eqs. (23) and (24) gives the plastic displacement Δ_p^{**} as

$$\Delta_p^{**} = (\phi_{u1} - \phi_i) \lambda_{p1} L_m^* D^2 \quad (25)$$

Eqs. (21), (22) and (25) can be substituted into Eq. (20) to give a relation between the displacement ductility factor and the curvature demand in the first plastic hinge:

$$\mu_\Delta = \frac{V_y}{V_u} + \frac{K_1}{K_2} \frac{(V_u - V_y)}{V_u} + \frac{\lambda_{p1} L_m^* D^2 (\phi_{u1} - \phi_i)}{\Delta_y} \quad (26)$$

By defining the coefficients $\alpha \equiv V_y / V_u = \Delta_{y1} / \Delta_y$ and $\beta \equiv \Delta_y / (\phi_y L_m^2)$, the curvature ductility factor $\mu_{\phi1}$ in the first plastic hinge is related to the displacement ductility factor μ_Δ by

$$\mu_\Delta = \alpha + \frac{K_1}{K_2} (1 - \alpha) + \frac{\lambda_{p1}}{\beta L_m^*} (\mu_{\phi1} - \mu_{\phi i}) \quad (27)$$

where $\mu_{\phi1}$ is defined as $\mu_{\phi1} \equiv \phi_{u1} / \phi_y$, and $\mu_{\phi i}$ is the curvature ductility demand in the first plastic hinge at the lateral displacement Δ_{y2} , which is defined as $\mu_{\phi i} \equiv \phi_i / \phi_y$.

The kinematic relation in Eq. (27) requires the determination of the curvature ductility $\mu_{\phi i}$, which involves the plastic rotation of the first plastic hinge at the lateral displacement Δ_{y2} . The plastic displacement Δ_p^* , which occurs from the first yield limit state to the second yield limit state, indicated as $\Delta_p^* = \Delta_{y2} - \Delta_{y1}$ in Figure 4, is associated with a plastic rotation θ_p^* in the first hinge. Assuming a uniform distribution of plastic rotation in the plastic hinge, the curvature ductility factor $\mu_{\phi i}$ is related to the plastic rotation θ_p^* by:

$$\mu_{\phi i} = \frac{\phi_i}{\phi_y} = 1 + \frac{\theta_p^*}{\phi_y L_{p1}} \quad (28)$$

The plastic rotation θ_p^* in Eq. (28) can be obtained using the expression for pile head rotation, as given in Eq. (5) for cohesive soils and Eq. (11) for cohesionless soils. By replacing the numerator $\Delta - \Delta_{y1}$ by Δ_p^* in Eq. (5) and (11), the plastic rotation θ_p^* can be written as:

$$\theta_p^* = \frac{\Delta_p^*}{\eta L_m} \quad (29)$$

where the coefficient η is defined as $\eta \equiv \sqrt{2} R_c / L_m$ for cohesive soils and $\eta \equiv 1.5 R_n / L_m$ for cohesionless soils. From the idealized tri-linear response shown in Figure 4, the plastic displacement Δ_p^* in Eq. (29) is related to the lateral strength and reduced stiffness of soil-pile system, i.e.

$$\Delta_p^* = \frac{V_u - V_y}{K_2} = \frac{K_1}{K_2} \frac{V_u - V_y}{K_1} \quad (30)$$

By substituting $V_y = \alpha V_u$ and $V_u / K_1 = \Delta_y = \beta \phi_y L_m^2$ into Eq. (30), Δ_p^* can be re-written as

$$\Delta_p^* = \frac{K_1}{K_2} \beta \phi_y L_m^2 (1 - \alpha) \quad (31)$$

The combination of Eqs. (28), (29) and (31) allows the curvature ductility μ_{ϕ_i} to be determined:

$$\mu_{\phi_i} = 1 + \frac{K_1}{K_2} \frac{\beta L_m^*}{\eta \lambda_{p1}} (1 - \alpha) \quad (32)$$

where L_m^* is the normalized depth to the second plastic hinge and λ_{p1} is the normalized plastic hinge length of the first hinge. Upon the determination of the intermediate curvature ductility factor, i.e. μ_{ϕ_i} in Eq. (32), the ultimate curvature ductility demand μ_{ϕ_1} in the first plastic hinge can be determined using Eq. (27) for a given displacement ductility factor μ_{Δ} .

Damage assessment of fixed-head piles also requires an estimation of the curvature ductility demand in the second plastic hinge, even though the curvature ductility demand would likely be smaller than that of the first plastic hinge. Similar to Eq. (24) for the first plastic hinge, the rotation θ_p^{**} due to the plastic displacement of Δ_p^* may be written in terms of the ultimate curvature demand ϕ_{u2} in the second hinge:

$$\theta_p^{**} = (\phi_{u2} - \phi_y) L_{p2} \quad \text{for } \phi_{u2} \geq \phi_y \quad (33)$$

where L_{p2} is the equivalent plastic hinge length of the second hinge. The combination of Eqs. (23) and (33) gives the plastic displacement Δ_p^{**} as

$$\Delta_p^{**} = (\phi_{u2} - \phi_y) \lambda_{p2} L_m^* D^2 \quad (34)$$

where $\lambda_{p2} \equiv L_{p2} / D$ is the normalized plastic hinge length of the second hinge. Following the same approach for the first plastic hinge, Eqs. (20), (21), (22) and (34) can be solved simultaneously to obtain the relation between the displacement ductility factor μ_{Δ} and the curvature ductility demand μ_{ϕ_2} :

$$\mu_{\Delta} = \alpha + \frac{K_1}{K_2} (1 - \alpha) + \frac{\lambda_{p2}}{\beta L_m^*} (\mu_{\phi_2} - 1) \quad (35)$$

where $\mu_{\phi_2} \equiv \phi_{u2} / \phi_y$ is the curvature ductility demand in the second plastic hinge. Note that Eq. (35) is similar to the kinematic relation for the first plastic hinge in Eq. (27), except that the plastic hinge length is different and the curvature ductility demand at lateral displacement Δ_{y2} is equal to unity for the second plastic hinge.

In order to ensure a good performance of a pile-supported foundation, the ultimate displacement imposed on the pile may be limited to a design displacement. If the design displacement is sufficiently large to cause inelastic deformation in both plastic hinges, the curvature ductility demand can be predicted using the kinematic relation of Eqs. (27) and (35). However, in the case of a small lateral displacement where the limiting design displacement Δ_u is less than the displacement at the formation of the second plastic hinge Δ_{y2} (but larger than Δ_{y1}), only one plastic hinge will form at the pile head. In this case, the kinematic relation will be different from that given by Eq. (27). In order to derive the kinematic relation for this condition, the displacement ductility factor μ_{Δ} may be written as:

$$\mu_{\Delta} \equiv \frac{\Delta_u}{\Delta_y} = \frac{\Delta_{y1}}{\Delta_y} + \frac{\Delta'_p}{\Delta_y} \quad (36)$$

where Δ_y is the elasto-plastic yield displacement as before, and Δ'_p is the plastic displacement, which is less than or equal to Δ_p^* . Similar to Eq. (29), the plastic displacement Δ'_p can be related to the plastic rotation of the first hinge θ'_p by

$$\Delta'_p = \theta'_p \eta L_m \quad (37)$$

where the coefficient η has been defined previously for cohesive and cohesionless soils. By writing the plastic rotation as $\theta'_p = (\phi_{u1} - \phi_y)L_{p1}$, where ϕ_{u1} is the ultimate curvature in the first plastic hinge, the displacement ductility factor μ_Δ in Eq. (36) can be written as

$$\mu_\Delta = \frac{\Delta_{y1}}{\Delta_y} + \frac{\eta L_{p1} L_m (\phi_{u1} - \phi_y)}{\Delta_y} \quad (38)$$

Substituting $\alpha = \Delta_{y1} / \Delta_y$ and $\Delta_y = \beta \phi_y L_m^2$ into Eq. (38), the relation between the displacement ductility factor μ_Δ and curvature ductility factor $\mu_{\phi1}$ for $\Delta_{y1} \leq \Delta_u \leq \Delta_{y2}$ is:

$$\mu_\Delta = \alpha + \frac{\eta \lambda_{p1}}{\beta L_m^*} (\mu_{\phi1} - 1) \quad (39)$$

where $\mu_{\phi1} \equiv \phi_{u1} / \phi_y$. The set of equations, namely Eqs. (27), (35) and (39), allows a full range of curvature ductility demand for fixed-head piles to be estimated.

Plastic Hinge Length of Fixed-Head Concrete Piles

The curvature demand in the yielding region of a pile is related to the equivalent plastic hinge length of the pile. Studies of bridge columns or extended pile-shafts have resulted in empirical expressions for the equivalent plastic hinge length. For the case of fixed-head piles, it is reasonable to assume that the length of the first plastic hinge is similar to the plastic hinge length of a fixed-based bridge column, since the first plastic hinge of the pile forms against a supporting member. In this case, the equivalent plastic hinge length L_{p1} of the pile is assumed to be the same as that of a fixed-based column except that the height of the column is replaced by one-half of the distance to the second hinge. This approach is based on the assumption that the bending moment in the upper region of fixed-head piles is similar to the reversed moment distribution in a laterally loaded column with full fixity at both ends. More specifically, the equivalent plastic hinge length for the first hinge of the fixed-head pile is taken from that proposed by Priestley et al. [9]:

$$L_{p1} = 0.04L_m + 0.022f_{ye}d_{bl} \geq 0.044f_{ye}d_{bl} \quad (40)$$

where f_{ye} is the expected yield strength of the reinforcing steel (in MPa units) and d_{bl} is the diameter of the longitudinal reinforcement of the pile. The equivalent plastic hinge length of the first plastic hinge, however, should not be taken as greater than the pile diameter. For the second plastic hinge, the spread of curvature will be more significant than that of the first plastic hinge. In this paper, the equivalent plastic hinge length for the second plastic hinge is taken from the plastic hinge length for extended pile-shafts with a zero above-ground height, as proposed by Chai [10]. In this case, a plastic hinge length of $L_{p2} = D$, or a normalized plastic hinge length of $\lambda_{p2} = 1.0$, is appropriate for the second plastic hinge.

ILLUSTRATIVE EXAMPLE

To illustrate the use of the analytical model, consider the following reinforced concrete fixed-head pile embedded in two different soils, which are classified according to NEHRP [3] as: (1) class E site with cohesive soils, and (2) class C site with cohesionless soils. The pile has a diameter of $D = 0.61$ m and an embedded length of 22 m, as shown in Figure 5. The following parameters are assumed for the pile: (i) the longitudinal reinforcement is provided by 12 # 25 bars, resulting in a longitudinal steel ratio of 0.020; (ii) the transverse reinforcement is provided by #13 spiral at a pitch of 75 mm, resulting in a confining steel ratio of 0.015; (iii) a concrete cover of 75 mm is used for the transverse spiral of the pile; (iv) the expected concrete compressive strength, as suggested by ATC-32 [6], is $f'_{ce} = 1.3f'_c = 44.8$ MPa; and (v) the longitudinal and transverse steel are provided by grade A706 steel with a expected yield strength $f_{ye} = 475$ MPa. The pile is subjected to an axial compression of 2000 kN or $0.2 f'_c A_g$.

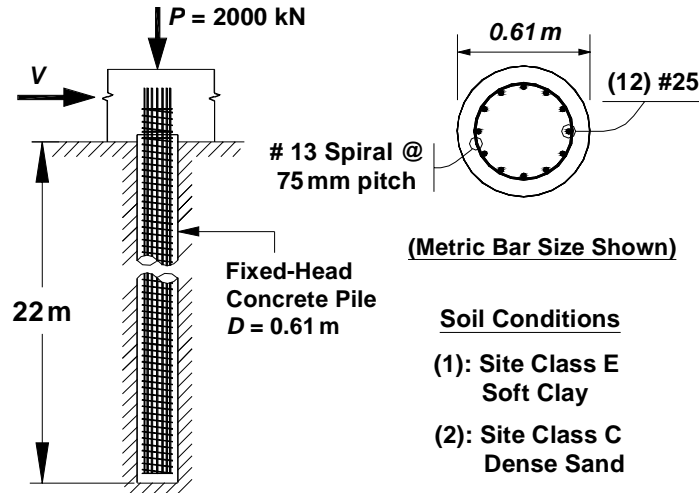


Figure 5. Details of a fixed-head pile

The moment-curvature response of the pile section may be idealized by an elasto-plastic response. In this case, the effective flexural rigidity of the pile is $EI_e = 1.029 \times 10^5 \text{ kN-m}^2$, and the equivalent elasto-plastic yield curvature is $\phi_y = 0.0079 \text{ rad/m}$. The ultimate bending moment of the pile, based on the elasto-plastic idealization, is $M_u = 809.9 \text{ kN-m}$. As a means for ensuring a good seismic performance of a structure, studies have suggested that damage can be controlled by limiting the strain values in the critical regions. For example, Kowalsky [11] suggested a damage-control strain of 0.018 for the extreme compressive fiber of the confined concrete core, or 0.060 for the extreme tension fiber of longitudinal steel. Following this suggestion for damage-control of fixed-head piles, the limiting curvature of the pile in this example is $\phi_u = 0.126 \text{ rad/m}$, which will be taken as the ultimate curvature of the section. Thus for the level of confining steel provided for the pile, the curvature ductility capacity is $(\mu_\phi)_{cap} = 16.0$. To demonstrate the applicability of the model, the curvature ductility demand will be estimated for a range of imposed displacement ductility factor up to 4.

Example 1: Soft Clay in Site Class E

The lateral response of the fixed-head pile in this example will be assessed for a cohesive soil, classified as profile type S_E or soft clay per NEHRP [3]. The effective unit weight of the soft clay is taken as $\gamma' = 17.5 \text{ kN/m}^3$ and the undrained shear strength is taken as $s_u = 35 \text{ kPa}$. From Eq. (6), the modulus of horizontal subgrade reaction is $k_h = 2345 \text{ kN/m}^2$. It should be noted that the soil stiffness estimated by Eq. (6) is intended for analyses at the working load level. For assessment of curvature ductility demand, however, the soil stiffness should correspond to the first yield limit state of the pile. Thus the soil stiffness that is appropriate for curvature ductility assessment should strictly be reduced since softening of the soil would have occurred upon first yielding of the pile. Currently no recommendation exists for the appropriate level of modification, and as such, the lateral stiffness of the soil predicted by Eq. (6) will be used in this example without reduction to illustrate the procedure. For $k_h = 2345 \text{ kN/m}^2$ and $EI_e = 1.029 \times 10^5 \text{ kN-m}^2$, the characteristic length of the pile is $R_c \equiv \sqrt[4]{EI_e / k_h} = 2.57 \text{ m}$. The critical depth of the pile, beyond which the ultimate lateral resistance of soil remains constant, is $x_r = 1.75 \text{ m}$, or corresponding to a critical depth coefficient of $\psi_r = 2.87$, as estimated from Eq. (13).

The initial lateral stiffness of the soil-pile system, as calculated from Eq. (1), is $K_1 = 8536 \text{ kN/m}$, whereas the reduced lateral stiffness, due to the first plastic hinge formation, is $K_2 = 4268 \text{ kN/m}$, as calculated from Eq. (4). The ratio of the two lateral stiffness coefficients is $K_1 / K_2 = 2.0$. From Eqs. (2) and (3), the lateral displacement and force at the first yield limit state are $\Delta_{y1} = 0.052 \text{ m}$ and $V_y = 445 \text{ kN}$, respectively.

Using a normalized flexural strength of $M_u^* = M_u / (s_u D^3) = 102.0$ and a critical depth coefficient of $\psi_r = 2.87$, the normalized depth to the second plastic hinge may be obtained by solving Eq. (14), which gives $L_m^* = 6.27$, or an actual depth of $L_m = 3.83$ m. The corresponding normalized lateral strength may be estimated by Eq. (15), which gives $V_u^* = 56.1$, or an actual lateral strength of $V_u = 730$ kN. From Eqs. (21) and (22), the elasto-plastic yield displacement is $\Delta_y = 0.086$ m and the lateral displacement at the formation of the second plastic hinge is $\Delta_{y2} = 0.119$ m. The curvature ductility demand depends on the ratio between V_y and V_u , which is represented by the coefficient of $\alpha = V_y / V_u = 0.61$. Using an elasto-plastic yield displacement of $\Delta_y = 0.086$ m, an elasto-plastic yield curvature of $\phi_y = 0.0079$ rad/m and the depth to the second plastic hinge of $L_m = 3.83$ m, the coefficient is $\beta = \Delta_y / (\phi_y L_m^2) = 0.74$. For $R_c = 2.57$ m and $L_m = 3.83$ m, the coefficient η , which is defined as $\eta = \sqrt{2} R_c / L_m$ for cohesive soils, is equal to 0.95. For this example, the equivalent plastic hinge length of the first plastic hinge of the pile is taken as $L_{p1} = 0.52$ m from Eq. (40), which corresponds to a normalized length of $\lambda_{p1} = 0.86$, while the plastic hinge length for the second plastic hinge is taken as $L_{p2} = D = 0.61$ m, which corresponds to a normalized length of $\lambda_{p2} = 1$. The curvature ductility demand μ_{ϕ_i} in the first plastic hinge at the lateral displacement Δ_{y2} is $\mu_{\phi_i} = 5.46$, as calculated from Eq. (32). The substitution of $\alpha = 0.61$, $\beta = 0.74$, $\eta = 0.95$, $\lambda_{p1} = 0.86$ and $L_m^* = 6.27$ into Eq. (39) gives the kinematic relation for small lateral displacements where only one plastic hinge forms. The same set of values plus $K_1 / K_2 = 2.0$, $\lambda_{p2} = 1$ and $\mu_{\phi_i} = 5.46$ can be substituted into Eqs. (27) and (35) for the case of large lateral displacement where both plastic hinges form.

The resulting kinematic relations for the first and second plastic hinges are plotted in Figure 6(a). It can be seen that the curvature ductility factor increases linearly with the displacement ductility factor for both plastic hinges. The slope of the straight line for the first plastic hinge is greater than that for the second plastic hinge due to the shorter length of the first plastic hinge. In the small displacement range where only one plastic hinge forms, i.e. $\mu_{\Delta} < 1.39$, the slope of the line is also slightly different from the slope where two plastic hinges form. For a curvature ductility capacity of 16.0 as estimated for the pile section, the result in Figure 6(a) indicates that the fixed-head pile can tolerate a displacement ductility factor of 3.33. Note that for a displacement ductility factor of $\mu_{\Delta} = 1$, the curvature ductility demand in the first plastic hinge is $\mu_{\phi_1} = 3.23$. The reason for the curvature ductility factor greater than unity is due to the definition of the elasto-plastic yield displacement Δ_y , which is larger than the lateral displacement to cause first yield of the pile Δ_{y1} .

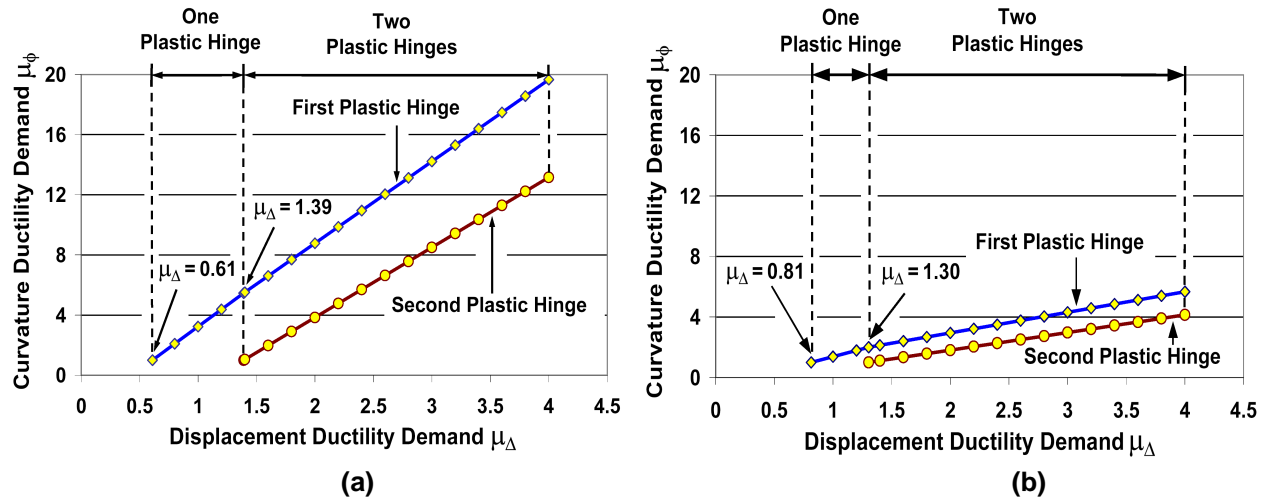


Figure 6. Kinematic relation for a fixed-head pile embedded in the (a) S_E cohesive soil (b) S_C cohesionless soil

Example 2: Dense Sand in Site Class C

The same fixed-head pile is analyzed for a cohesionless soil classified as profile type S_C per NEHRP (2001). The sand is assumed to be dry with an effective unit weight of $\gamma' = 20.5 \text{ kN/m}^3$ and an internal friction angle of $\bar{\phi} = 42^\circ$. For the selected friction angle, the passive soil pressure coefficient is $K_p = (1 + \sin \bar{\phi}) / (1 - \sin \bar{\phi}) = 5.04$. The rate of increase of modulus of horizontal subgrade reaction, which is extrapolated from the above-water curve of Figure 2, is $n_h = 27000 \text{ kN/m}^3$. Although the soil stiffness should similarly be modified for assessment of curvature ductility demand, as discussed previously for cohesive soils, the soil stiffness estimated from Figure 2 will also be used without modification to illustrate the procedure. Using the same flexural rigidity of $EI_e = 1.029 \times 10^5 \text{ kN-m}^2$ and a soil stiffness of $n_h = 27000 \text{ kN/m}^3$, the characteristic length of the soil-pile system is $R_n \equiv \sqrt[5]{EI_e / n_h} = 1.31 \text{ m}$.

The lateral stiffness of the soil-pile system, as estimated from Eqs. (7) and (10), is $K_1 = 49801 \text{ kN/m}$ and $K_2 = 18906 \text{ kN/m}$, giving a stiffness ratio of $K_1 / K_2 = 2.6$. The lateral displacement and force required to develop the first plastic hinge are $\Delta_{y1} = 0.013 \text{ m}$ and $V_y = 669.3 \text{ kN}$, as calculated from Eqs. (8) and (9), respectively. Using the normalized flexural strength of $M_u^* = M_u / (K_p \gamma' D^4) = 56.56$, the normalized depth to the second plastic hinge is $L_m^* = 4.84$ from Eq. (18), which corresponds to an actual depth of $L_m = 2.95 \text{ m}$. The normalized lateral strength of the soil-pile system is $V_u^* = 35.09$ from Eq. (19), giving an actual lateral strength of $V_u = 823.6 \text{ kN}$. The elasto-plastic yield displacement may be calculated from Eq. (21), which is $\Delta_y = 0.017 \text{ m}$. The lateral displacement at the second yield limit state is $\Delta_{y2} = 0.022 \text{ m}$, as calculated from Eq. (22). Using $V_y = 669.3 \text{ kN}$ and $V_u = 823.6 \text{ kN}$, the coefficient $\alpha = V_y / V_u$ is equal to 0.81. For $\Delta_y = 0.017 \text{ m}$, $L_m = 2.95 \text{ m}$, and $\phi_y = 0.0079 \text{ rad/m}$, the coefficient is $\beta = \Delta_y / (\phi_y L_m^2) = 0.24$. Using $R_n = 1.31 \text{ m}$ and $L_m = 2.95 \text{ m}$, the coefficient η for cohesionless soils is $\eta = 1.5 R_n / L_m = 0.66$. The normalized plastic hinge lengths are the same as before for the cohesive soil, i.e. $\lambda_{p1} = 0.86$ and $\lambda_{p2} = 1$. The curvature ductility μ_{ϕ_i} in the first plastic hinge at the lateral displacement Δ_{y2} is $\mu_{\phi_i} = 2.01$, as estimated from Eq. (32). Substituting $\alpha = 0.81$, $\beta = 0.24$, $\eta = 0.66$, $\lambda_{p1} = 0.86$, and $L_m^* = 4.84$ into Eq. (39) gives the kinematic relation for the case of small lateral displacement where only one plastic hinge forms. The same set of values plus $K_1 / K_2 = 2.6$, $\lambda_{p2} = 1$ and $\mu_{\phi_i} = 2.01$ can be substituted into Eqs. (27) and (35) for the case where both plastic hinges form. The resulting kinematic relations are plotted in Figure 6(b) for comparison with the case of soft clay.

The curvature ductility demand for the pile in dense sand follows the same trend as the soft clay with linearly increasing curvature ductility factor for increased displacement ductility factor. For a given displacement ductility factor, however, the curvature ductility demand in dense sand is significantly smaller than the curvature ductility demand in soft clay. For example, at a displacement ductility factor of $\mu_\Delta = 4$, the curvature ductility demand is $\mu_{\phi_i} = 5.68$ for the case of dense sand compared to the curvature ductility demand of $\mu_{\phi_i} = 19.65$ for soft clay. Although not plotted in Figure 6(b), the estimated curvature ductility capacity of 16.0 for the pile section would correspond to a displacement ductility factor of $\mu_\Delta = 11.5$, which is significantly larger than the displacement ductility normally adopted for design.

PRELIMINARY RESULTS FOR DAMAGE ASSESSMENT

Under lateral seismic loads, damage to piles is often related to the curvature ductility demand in the critical regions of the pile. Consequently, the curvature ductility demand is used as an indicator of pile damage in this paper. The curvature ductility demand however depends not only on the displacement ductility imposed on the pile, but also on the properties of the soil. Since a wide range of soil conditions

exist in practice, seismic performance of a fixed-head pile may vary significantly depending on the site condition. In this section, the performance of a fixed-head is assessed for a wide range of soils, from profile type S_E to profile type S_C per NEHRP [3] or ATC-40 [4]. The assessment is made using the same pile details as presented in the previous section. The variation in soil profile types is achieved by varying the undrained shear strength from $s_u = 20$ to 250 kN/m² for cohesive soils and by varying the relative density from $D_r = 15\%$ to 90% for cohesionless soils. The curvature ductility demand in the fixed-head pile is calculated for displacement ductility factors of $\mu_\Delta = 2.5$ and $\mu_\Delta = 3$.

The resulting curvature ductility demand for the first and second plastic hinges of the fixed-head pile is plotted in Figure 7. Figure 7(a) shows the curvature ductility demand versus the undrained shear strength of cohesive soils. Note that the soil profile type is also labeled on the horizontal axis in the figure. It can be seen that the curvature ductility demand is relatively constant for a given displacement ductility factor. For an imposed displacement ductility factor of $\mu_\Delta = 3$, for example, the curvature ductility demand in the first plastic hinge increases slightly from $\mu_{\phi 1} = 13.4$ at an undrained shear strength of $s_u = 20$ kN/m² to $\mu_{\phi 1} = 14.9$ at an undrained shear strength of $s_u = 100$ kN/m², and then decreases slightly to $\mu_{\phi 1} = 14.6$ when the undrained shear strength increases to $s_u = 250$ kN/m². For soft cohesive soils (soil type S_E), the variation of curvature ductility demand in the second plastic hinge is less compared to that of the first plastic hinge. For the pile analyzed in this example, the curvature ductility capacity of $(\mu_\phi)_{cap} = 16.0$ is adequate for a large range of cohesive soils.

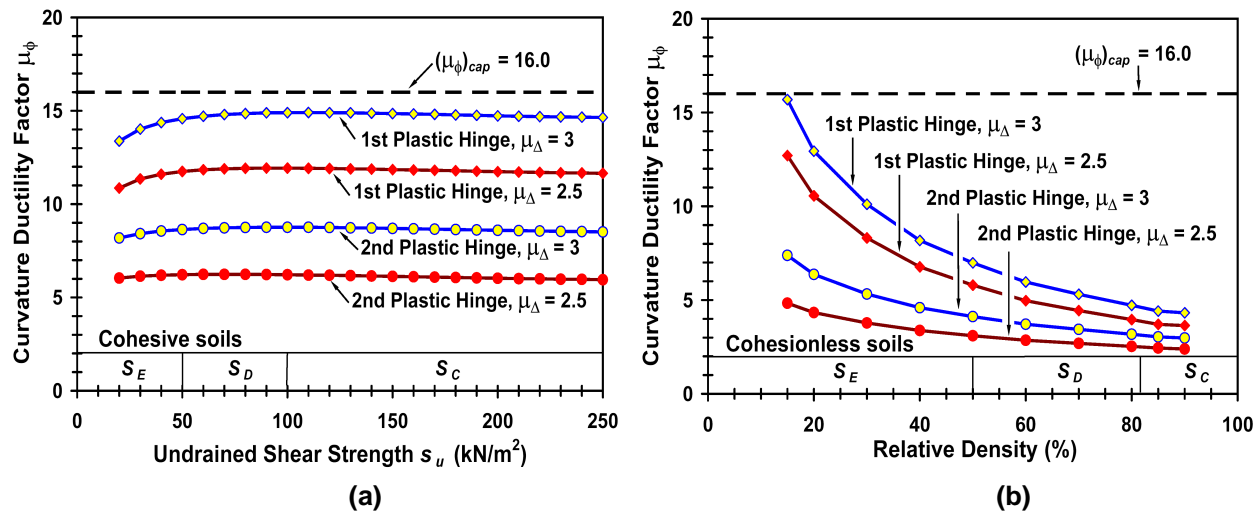


Figure 7. Curvature ductility demand of a fixed-head pile embedded in profile type S_C to S_E (a) cohesive soils (b) cohesionless soils

The curvature ductility demand for the same pile embedded in cohesionless soils is shown in Figure 7(b). The curvature ductility demand decreases with increased soil stiffness, as signified by the increase in relative density, especially for the first plastic hinge. The decrease in curvature ductility demand is more significant for piles embedded in S_E cohesionless soils. Similar to the trend observed for cohesive soils, the decrease in curvature ductility demand in the second plastic hinge is smaller than that of the first plastic hinge. The curvature ductility capacity of $(\mu_\phi)_{cap} = 16.0$ is adequate for a large range of cohesionless soils for an imposed displacement ductility factor of $\mu_\Delta = 3$. It is important to note that the results presented in Figure 7 are preliminary since they have been calculated without a modification in the soil stiffness for both cohesive and cohesionless soils. An adjustment of the soil stiffness however may

lead to an increased curvature ductility demand in the pile. Further research into the appropriate level of soil stiffness modification for curvature ductility demand estimation is warranted.

CONCLUSIONS

Seismic design of deep foundations should include an assessment of the curvature ductility demand in the potential plastic hinge region of the pile. In this paper, an analytical model is developed for assessing the curvature ductility demand of fixed-head piles embedded in cohesive and cohesionless soils. The model is useful for performance-based design since local damage can be controlled by limiting the curvature ductility demand in the plastic hinges of the pile. For the proposed model, the lateral response is characterized by a linear elastic response, followed by first yielding of the pile at the pile head, and then by a full plastic mechanism after the formation of the second plastic hinge. The elastic response of the pile and its first yield limit state are determined using classical solutions of a flexural element supported by an elastic Winkler foundation. The ultimate lateral strength, as defined by a fully plastic mechanism, is determined using the flexural strength of the pile and the ultimate pressure distribution of the soil. A kinematic relation between the global displacement ductility factor and local curvature ductility demand is developed by assuming a concentrated plastic rotation in both plastic hinges. The kinematic relation indicates that the curvature ductility demand depends on the ratio of the first yield lateral force to ultimate lateral force, the initial stiffness to post first yield stiffness ratio, the depth to the second plastic hinge, and the plastic hinge length of the pile. The versatility of the proposed model is illustrated using a fixed-head reinforced concrete pile embedded in two different soil types, as classified in current US building codes. Although results presented in this paper are preliminary, the model is nonetheless shown to be capable of predicting the local ductility demand for a wide range of pile and soil properties.

REFERENCES

1. Poulos HG, Davis EH. "Pile foundation analysis and design." New York: Wiley-Interscience, 1980.
2. Davisson MT. "Lateral load capacity of piles." Highway Research Record 1970; 333: 104-112.
3. NEHRP. "NEHRP recommended provisions for seismic regulations for new buildings and other structures, FEMA 368." Washington, D.C., 2001.
4. Applied Technology Council ATC-40. "Seismic evaluation and retrofit of concrete buildings." Redwood City, California, 1996.
5. Matlock H, Reese LC. "Generalized solutions for laterally loaded piles." Journal of Soil Mechanics and Foundations Division (ASCE) 1960; 86(SM5): 63-91.
6. Applied Technology Council ATC-32. "Improved seismic design criteria for California bridges: provisional recommendations." Redwood City, California, 1996.
7. Reese LC, Van Impe WF. "Single piles and pile groups under lateral loading." Rotterdam: Balkema, 2001.
8. Broms BB. "Lateral resistance of piles in cohesionless soils." Journal of Soil Mechanics and Foundations Division (ASCE) 1964; 90(SM3): 123-156.
9. Priestley MJN, Seible F, Calvi GM. "Seismic design and retrofit of bridges." New York: Wiley-Interscience, 1996.
10. Chai YH. "Flexural strength and ductility of extended pile-shafts. I: Analytical model." Journal of Structural Engineering (ASCE) 2002; 128(5): 586-594.
11. Kowalsky MJ. "Deformation limit states for circular reinforced concrete bridge columns." Journal of Structural Engineering (ASCE) 2000; 126(8): 869-878.